Chinese Chemical Letters 37 (2026) 112026

Contents lists available at ScienceDirect

Chinese Chemical Letters

journal homepage: www.elsevier.com/locate/cclet

Engineering semiconductor/electrocatalyst interface for efficient photoelectrochemical water splitting

Fangming Zhao, Xingming Ning*, Li Xu, Pei Chen*, Zhongwei An, Xinbing Chen*

Key Laboratory of Applied Surface and Colloid Chemistry (MOE), Shaanxi Key Laboratory for Advanced Energy Devices, Shaanxi Engineering Laboratory for Advanced Energy Technology, International Joint Research Center of Shaanxi Province for Photoelectric Materials Science, School of Materials Science and Engineering, Shaanxi Normal University, Xi'an 710119, China

ARTICLE INFO

Article history:
Received 29 April 2025
Revised 28 August 2025
Accepted 26 October 2025
Available online 27 October 2025

Keywords:
Photoelectrochemical water splitting
Interface charge recombination
Hole transporter
Charge transfer kinetics
Charge separation

ABSTRACT

Loading transition metal oxyhydroxides (TMOH) electrocatalyst on semiconductors (SC) improves the photoelectrochemical (PEC) water splitting performance. However, the inevitable interface charge recombination between SC and TMOH hinders the PEC efficiency. Herein, differing from the conventional charge transfer process, a novel charge modulation layer, *i.e.*, Ce-CoO_x, like a "hole transporter" has been incorporated into the SC/TMOH system. A series of electrochemical characterizations confirm that the "hole transporter" can directly and rapidly transfer holes from $BiVO_4$ to FeNiOOH, resulting in a highly efficient charge separation. As expected, the $BiVO_4$/Ce-CoO_x/FeNiOOH photoanode presents a desirable photocurrent of 6.0 mA/cm^2 and good stability. More importantly, the smart approach can also be extended to $BiVO_4$/Ce-NiO_x/FeNiOOH system, proving its universality. This work opens up a new avenue for designing efficient photoanode for PEC water splitting.

© 2026 Published by Elsevier B.V. on behalf of Chinese Chemical Society and Institute of Materia Medica, Chinese Academy of Medical Sciences.

Solar-driven hydrogen (H_2) production is widely regarded as a pivotal strategy to address environmental challenges and global energy [1–4]. Since the pioneering discovery of TiO_2 photoanodes in 1972 [5], semiconductor (SC) based photoelectrochemical (PEC) water splitting has garnered significant attention [6–11]. Nevertheless, these photoanodes, suffering from significant charge recombination and slow oxygen evolution reaction (OER) kinetics, result in photocurrent densities far below theoretical limits under AM 1.5 G illumination. Recently, numerous efforts have been made to enhance PEC performance, including heterojunction engineering [12], defect modulation [13], elemental doping [14], and electrocatalyst loading [15].

Among the strategies mentioned above, deposition of efficient OER electrocatalyst, namely, transition metal oxyhydroxide (TMOH), on photoanodes has been treated as a promising approach to improve PEC water splitting performance [16–19]. However, only integrating high-activity TMOH often fails to achieve the desired photocurrent density due to inefficient hole extraction at the SC/TMOH interface, which will inevitably lead to interfacial charge recombination [14,20–24]. Addressing this challenge necessitates innovative strategies to effectively boost interfacial charge separation.

Introducing an interfacial regulation layer (IRL) at the SC/TMOH interface significantly improves charge separation. For instance, $Ni(OH)_2$ [25], CoOOH [26], and $Ni(OH)_x/CoO_x$ [27] act as efficient IRLs by storing or transferring holes. Specifically, CoO_x, as a p-type semiconductor, can adhere tightly to BV, forming strong interfacial bonding between CoO_x and BV, which can efficiently boost charge transfer across the formed interface [28]. Building on these advances, this study constructs a novel SC/TMOH system using interfacial regulation layers (Ce-CoO_x and Ce-NiO_x) to optimize hole transfer kinetics. $BiVO_4$ (named BV) is selected as the photoanode for its narrow bandgap (*ca.* 2.4 eV), suitable band alignment, and abundance [29–33]. Given their tunable 4f energy levels and variable 4f valence states, rare-earth elements (*e.g.*, Ce) are posited to modulate the electronic structure [34–36]. Meanwhile, for a highly efficient surface catalytic reaction, NiFe-based oxyhydroxides (*i.e.*, FeNiOOH) have attracted extensive attention owing to their natural abundance, excellent stability, and exceptional OER activity under alkaline conditions [37–38].

In this work, the designed IRL directly facilitates hole migration from BV to FeNiOOH, curbing recombination and prolonging carrier lifetimes. A series of experimental results demonstrate that the BV/Ce-CoO_x/FeNiOOH photoanode achieves a photocurrent density of 6.0 mA/cm^2 at 1.23 V *vs.* RHE under AM 1.5 G illumina-

* Corresponding authors.
E-mail addresses: ningxingming@snnu.edu.cn (X. Ning), chenpei@snnu.edu.cn (P. Chen), chenxinbing@snnu.edu.cn (X. Chen).

https://doi.org/10.1016/j.cclet.2025.112026
1001-8417/© 2026 Published by Elsevier B.V. on behalf of Chinese Chemical Society and Institute of Materia Medica, Chinese Academy of Medical Sciences.

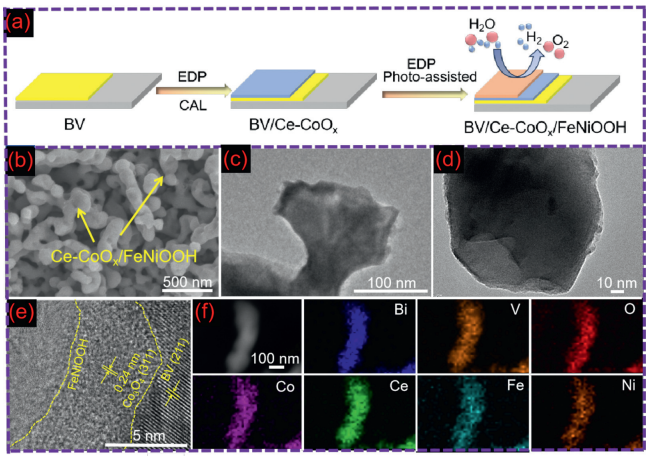


Fig. 1. (a) Fabrication process of the BV/Ce-CoO_x/FeNiOOH photoanode. (b) SEM images of BV/Ce-CoO_x/FeNiOOH. (c, d) TEM, (e) high-resolution TEM, (f) EDS mapping of BV/Ce-CoO_x/FeNiOOH.

tion (100 mW/cm^2) with outstanding stability. This enhancement is further validated in the BV/Ce-NiO_x/FeNiOOH system, proving the universality of this strategy. These findings highlight the hole transfer behavior in advancing solar H_2 production.

Fig. 1a demonstrates a flexible preparation process of the BV/Ce-CoO_x/FeNiOOH photoanode, and the BV array was synthesized through electrodeposition (EDP) followed by calcination. The structural and morphological properties were characterized by scanning electron microscopy (SEM, Fig. S1 in Supporting information) and transmission electron microscopy (TEM). Vermicular BV nanoarrays (with diameters of 150–200 nm) were uniformly coated on Fluorine-doped tin oxide (FTO) substrates. X-ray diffraction (XRD) confirms the monoclinic BV structure (JCPDS No. 14–0688, Fig. S2 in Supporting information) [31], while X-ray photoelectron spectroscopy (XPS, Fig. S3 in Supporting information) and Raman spectroscopy (Fig. S4 in Supporting information) together confirm the successful synthesis of BV.

The Ce-CoO_x layer were deposited on BV arrays *via* EDP followed by calcination (CAL), as evidenced by morphological characterization (Fig. S5 in Supporting information). The lack of detectable changes in crystalline phases in XRD patterns (Fig. S6 in Supporting information) and Raman spectra (Fig. S7 in Supporting information) indicates the formation of an ultrathin, homogeneously distributed covering layer. Furthermore, XPS, XRD, and Raman analyses have unambiguously confirmed the formation of BV/Ce-CoO_x (Figs. S7 and S8 in Supporting information).

This photo-assisted EDP strategy was successfully extended to fabricate BV/Ce-CoO_x/FeNiOOH and BV/FeNiOOH photoanodes (Figs. S9-S12 in Supporting information), demonstrating its versatility for TMOH deposition.

For the BV/Ce-CoO_x/FeNiOOH photoanode, we can observe a hierarchical architecture (a roughened BV surface compared to BV, Fig. 1b), where BV is sequentially coated with a Ce-CoO_x interlayer and an outer FeNiOOH layer, as evident by TEM images (Figs. 1c and d). Fig. 1e shows distinct lattice fringes in the BV region with a *d*-spacing of 0.29 nm, corresponding to the (211) planes. Additionally, a *d*-spacing of 0.24 nm, originating from Co_3O_4, is confirmed by XRD results (Fig. S8) and previous reports [39,40]. This clearly distinguishes the CoO_x layer from BV and FeNiOOH (which have an amorphous nature, as confirmed by XRD, Fig. S10). In the energy dispersive spectroscopy (EDS) mapping images (Fig. 1f), Bi and V elements are localized in the central region of BV/Ce-CoO_x/FeNiOOH. In contrast, Ce, Co, Ni, and Fe elements are homogeneously distributed across the entire composite, verifying the successful synthesis of BV/Ce-CoO_x/FeNiOOH, and this can also be confirmed by XPS results (Fig. S13 in Supporting information). An obvious positive shift is observed in the Bi 4f and V 2p peaks for BV/Ce-CoO_x/FeNiOOH compared to those for BV and BV/Ce-CoO_x, indicating the excellent charge transfer properties at the interfaces of BV, Ce-CoO_x, and FeNiOOH (Fig. S14 in Supporting information). Additionally, the ultrathin nature of both the Ce-CoO_x and FeNiOOH layers can still be evidenced by XRD patterns and Raman spectra (Fig. S15 in Supporting information).

The PEC water splitting performance of these BV based photoanodes was assessed in a traditional three-electrode system under AM 1.5 G illumination. As shown in Fig. 2a, the photocurrent response of the BV photoanode is relatively low, which is restricted by the severe charge recombination and the slow OER process. Notably, after functionalizing the BV photoanode with the Ce-CoO_x layer, the BV/Ce-CoO_x composite achieved a significant photocurrent enhancement of 3.4 mA/cm^2. This is likely attributed to the promotion of charge separation. In addition, when the surface of the BV photoanode is decorated with FeNiOOH, the PEC activity can be significantly enhanced. Specifically, the photocurrent increased to 4.0 mA/cm^2 at 1.23 V_{RHE} (Fig. 2a).

Regrettably, the conventional BV/FeNiOOH structure still has the problem of interfacial charge recombination. Interestingly, after introducing the Ce-CoO_x interlayer between BV and FeNiOOH, the optimized photocurrent density achieved a breakthrough increase, reaching 6.0 mA/cm^2 at 1.23 V_{RHE} (Fig. 2a, Figs. S16 and S17 in Supporting information). The applied bias photon-to-current efficiency (ABPE) calculated based on the photocurrent density curve shows that the BV/Ce-CoO_x/FeNiOOH reaches a peak efficiency of 1.8 % at 0.72 V_{RHE} (Fig. 2b), which is significantly better than that of BV/FeNiOOH (1.3 %, 0.72 V_{RHE}) and pristine BV (0.4 %, 0.82 V_{RHE}).

Furthermore, EIS was employed to investigate the charge transfer properties. According to the Nyquist plots and the fitting results (Fig. 2c and Table S1 in Supporting information), the corresponding charge transfer resistance (R_{ct}) exhibits the following trends: BV (1130 Ω) > BV/Ce-CoO_x (750 Ω) > BV/FeNiOOH (553 Ω) > BV/Ce-CoO_x/FeNiOOH (361 Ω), further demonstrating that the Ce-CoO_x layer significantly enhances hole transfer, as evidenced by the improved surface charge separation efficiency (Fig. 2d) and the increased incident photon-to-current conversion efficiencies (IPCE, Fig. S18 in Supporting information). To further confirm the charge separation ability and carrier dynamics, photoluminescence (PL) spectroscopy and time-resolved photoluminescence (TRPL) were conducted. As shown in Fig. 2e and Fig. S19 (Supporting information), the BV/Ce-CoO_x/FeNiOOH exhibits a prolonged carrier lifetime (*ca.* 3.53 ns, Table S2 in Supporting information) and reduced PL intensity, confirming efficient interfacial charge separation at the BV/FeNiOOH interface. Building on the aforementioned positive outcomes, we evaluated the PEC activity in comparison with that of previously reported BV-based photoanodes. As illustrated in Table S3 (Supporting information), our integrated system exhibits remarkable competitiveness.

Beyond high PEC water splitting efficiency, excellent photostability is a critical factor for practical applications. As shown in Fig. 2f, the bare BV photoanode exhibits a photocurrent density decline from 1.6 mA/cm^2 to 0.6 mA/cm^2 over 1 h under AM 1.5 G irradiation, suggesting significant photocorrosion of the pristine BV. On the contrary, the BV/Ce-CoO_x/FeNiOOH photoelectrode remains above 91 % after 3 h of operation, implying excellent photoactivity for PEC water splitting, which is attributed to the rapid hole transfer mediated by Ce-CoO_x.

To elucidate the origin of the improved PEC activity, UV-vis diffuse reflectance spectroscopy (DRS) analysis was performed. The overlapping absorbance results in Fig. S20 (Supporting information) indicate that "Ce-CoO_x" exerts a negligible impact on the sub-

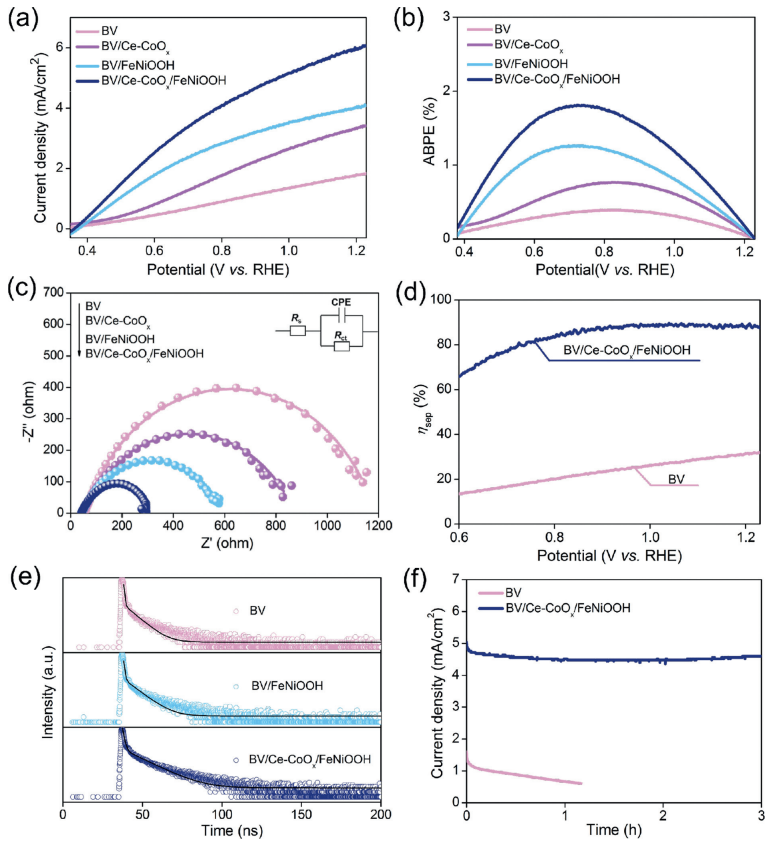


Fig. 2. (a) Linear-sweep voltametric (LSV) curves, (b) ABPE, (c) electrochemical impedance spectroscopy (EIS) for different photoanodes. (d) Charge separation efficiencies of different photoanodes. (e) TRPL of different samples. (f) *I-t* curves of different photoanodes.

stantial PEC improvement, as supported by the similar light harvesting efficiency (LHE, Fig. S20). Therefore, it can be inferred that the photocurrent enhancement primarily originates from interfacial charge separation. To further evaluate the separation of photogenerated charges, intensity-modulated photocurrent spectroscopy (IMPS) was employed. As depicted in Figs. 3a and b, K_{ct} stands for the charge transfer rate constant, whereas K_{rc} signifies the charge recombination rate constant. In Fig. 3c, pristine BV exhibits a substantially higher K_{rc} than K_{ct} due to pronounced charge recombination. When the FeNiOOH layer is integrated on BV, K_{ct} increases, yet K_{rc} remains dominant, as shown in Fig. 3c. This is mainly due to interfacial charge recombination occurring at the BV/FeNiOOH interface, as evidenced by the rapid photocurrent decay shown in Fig. S21 (Supporting information).

Upon the introduction of "Ce-CoO$_x$", the K_{ct} values far exceed the K_{rc} values, typically, the K_{ct} of BV/Ce-CoO$_x$/FeNiOOH is 4 times higher than that of BV/FeNiOOH. This implies that the interfacial charge recombination can be effectively inhibited, consistent with the charge transfer efficiency result (Fig. S22 in Supporting information) and the "slow" current decreasing trend (Fig. S16). Transient time ($\tau_d = 1/(2\pi f_{IMPS})$) shows the following trend: BV/Ce-CoO$_x$/FeNiOOH (0.42 ms) < BV/FeNiOOH (0.61 ms) < BV/Ce-CoO$_x$ (0.74 ms) < BV (0.89 ms) (Fig. S23, Table S4 in Supporting information), meaning that the Ce-CoO$_x$ boosts the hole transfer kinetics, consistent with the increasing value of K_{ct}.

Even though "Ce-CoO$_x$" has the capacity to inhibit interfacial charge recombination, it remains uncertain whether photogenerated holes are prone to transfer to the surface of the photoelectrode. Therefore, ($[Fe(CN)_6]^{3-}$/$[Fe(CN)_6]^{4-}$), a soft probe molecule, was employed to explore the charge transfer behavior (Fig. 3d). Under illumination, the BV/Ce-CoO$_x$/FeNiOOH sample exhibits a lower redox potential and a higher photocurrent density compared to pristine BV (Fig. 3e), demonstrating that more photogenerated holes from the valence band (VB) of BV are transferred to the surface for oxidation reactions, which correlates well with the low R_{ct} value (Fig. 3f) and high open circuit potential (OCP) values (Fig. S24 in Supporting information).

Even so, the fundamental reason for the improvement in PEC water splitting performance remains unknown. Previous studies identified two primary hole modulation strategies: (1) Passivation layers [41]; (2) storage layers [42]. To elucidate this, we conducted cyclic voltammetry (CV) on isolated Ce-CoO$_x$ components. Notably, Ce-CoO$_x$ exhibits near-elimination of redox peaks compared to pristine CoO$_x$ (Figs. S24 and S25 in Supporting information), indicating a fundamental shift in hole transfer mechanisms. Coupled with the fast K_{ct} value, high electrical conductivity (Fig. S26a in Supporting information), low R_{ct} value (Fig. S26b in Supporting information), and comparative tests on FeOOH (Fig. S26c in Supporting information), we can confirm that Ce-CoO$_x$ does not undergo the traditional charge transfer behavior but acts as an innovative "hole transporter" that modulates the charge transfer pathway. This engineered layer redirects holes through optimized transfer pathways to electrocatalytic surfaces, thereby achieving superior PEC performance (Fig. S26).

To validate the aforementioned hypothesis, we demonstrate that integrating Ce-NiO$_x$ as a "hole transporter" at the BV/FeNiOOH interface is a universal strategy to enhance hole separation (Figs. S27 and S28 in Supporting information). The results of LSV measurements show that, at 1.23 V_{RHE}, the photocurrent density of the BV/Ce-NiO$_x$/FeNiOOH photoanode is respectively higher than that of its BV/FeNiOOH and BV counterparts (Fig. 4a). The results of ABPE (Fig. 4b), EIS (Fig. 4c and Table S5 in Supporting information), and PL (Fig. S29 in Supporting information) support the enhanced PEC activity.

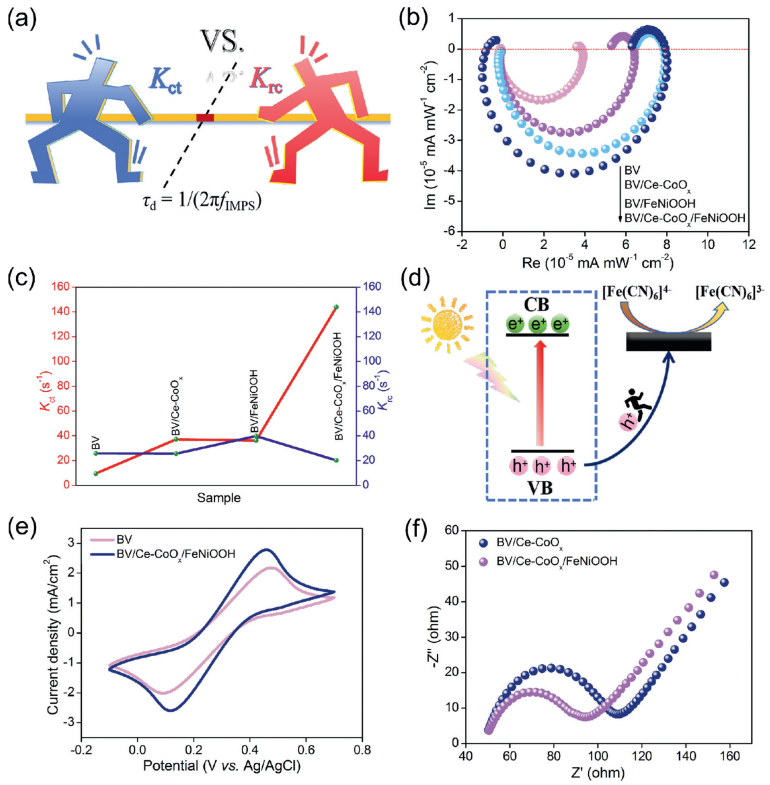


Fig. 3. (a) Principle of the IMPS setup. (b) IMPS responses for different photoanodes. (c) Charge transfer rate constant and recombination rate constant of different photoanodes. (d) The oxidation of soft probe molecules. (e) CV curves, (f) EIS curves of different photoanodes.

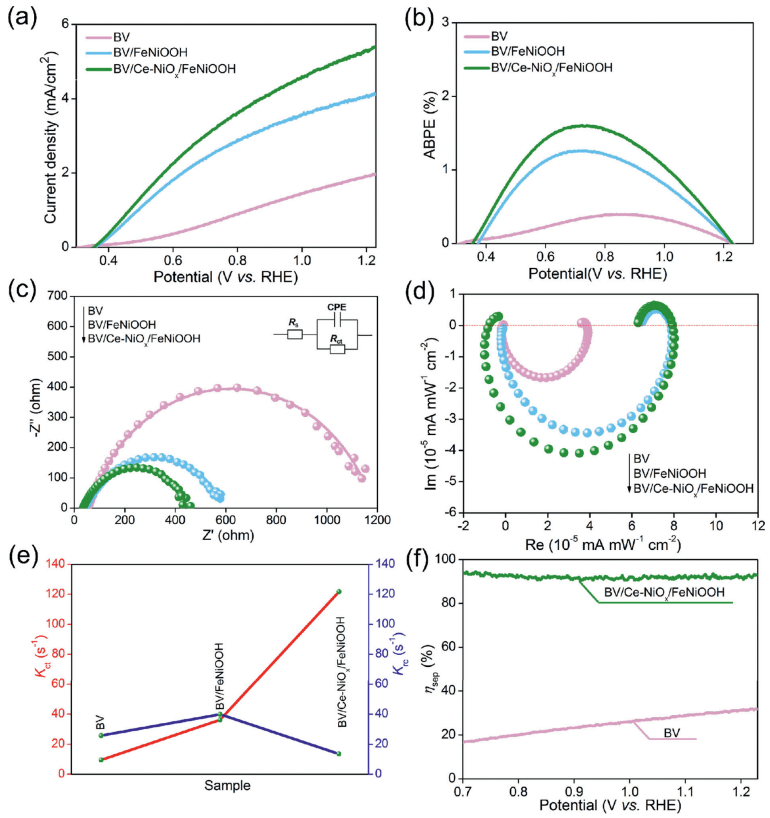


Fig. 4. (a) LSV curves, (b) ABPE, (c) EIS, (d) IMPS response of different samples. (e) Charge transfer rate constant and recombination rate constant. (f) Charge separation efficiencies of different samples.

Based on the DRS and LHE results (Fig. S30 in Supporting information), Ce-NiO_x still has a negligible impact on light absorption, while it positively affects interfacial charge separation, as evidenced by IMPS (Figs. 4d and e, Figs. S31 and S32, and Table S6 in Supporting information). We can further conclude that, like Ce-CoO_x, Ce-NiO_x also acts as a "hole transporter" capable of regulating charge transfer behavior, thereby enabling high PEC performance (Fig. 4f). This enhancement primarily stems from the suppression of interfacial recombination *via* rapid hole transfer.

In conclusion, we have successfully developed an interface engineering strategy to modulate the SC/TMOH interface, aiming to enhance the PEC activity of the BV/Ce-CoO_x/FeNiOOH integrated system for water splitting. A series of electrochemical characterizations demonstrate that the incorporation of a Ce-CoO_x interfacial mediator can effectively suppress charge recombination at the BV/FeNiOOH interface by modulating charge transfer pathway and accelerating hole transfer kinetics. Notably, BV/Ce-CoO_x/FeNiOOH exhibits the highest hole transfer kinetic rate constant of 143.92 s^{-1}, which is four times that of BV/FeNiOOH (36.22 s^{-1}). As expected, the optimized BV/Ce-CoO_x/FeNiOOH configuration delivers a remarkable photocurrent density of 6.0 mA/cm^2 at 1.23 V_{RHE}, alongside superior durability. More importantly, we have extended this strategy to other interface regulation layers, including Ce-NiO_x, thereby demonstrating the universality of this approach. This work provides a novel perspective on the design of prospective photoanodes for water splitting.

Declaration of competing interest

The authors declare that they have no known competing financial interests or personal relationships that could have appeared to influence the work reported in this paper.

CRediT authorship contribution statement

Fangming Zhao: Writing – review & editing, Writing – original draft, Methodology, Formal analysis, Data curation. **Xingming Ning:** Writing – review & editing, Writing – original draft, Methodology, Investigation, Funding acquisition. **Li Xu:** Writing – review & editing, Validation, Supervision, Methodology. **Pei Chen:** Writing – review & editing, Resources, Funding acquisition. **Zhongwei An:** Writing – review & editing, Resources, Methodology. **Xinbing Chen:** Writing – review & editing, Resources, Methodology, Funding acquisition.

Acknowledgments

The authors are thankful to the National Natural Science Foundation of China (Nos. 22202126, 52273186, and 51873100), International Joint Research Center of Shaanxi Province for Photoelectric Materials Science, the Science and Technology Innovation Team of Shaanxi Province (No. 2023-CXTD-27), San Qin Scholars Innovation Teams in Shaanxi Province, China, Fundamental Research Funds for the Central Universities (Nos. GK202403002, GK202202001).

Supplementary materials

Supplementary material associated with this article can be found, in the online version, at doi:10.1016/j.cclet.2025.112026.

References

[1] B. Liu, X. Wang, Y. Zhang, et al., Nat. Commun. 16 (2025) 2792.
[2] J. Ge, X. Wang, H. Tian, et al., Chin. Chem. Lett. 36 (2025) 109906.
[3] P. Zhang, B. Shen, X. Li, et al., Chin. Chem. Lett. 34 (2023) 108588.
[4] L. Gao, X. Zhong, J. Chen, et al., Chin. Chem. Lett. 34 (2023) 108085.
[5] A. Fujishima, K. Honda, Nature 238 (1972) 37.
[6] L. Yan, G. Dong, X. Huang, et al., Appl. Catal. B: Environ. Energy 345 (2024) 123682.
[7] G. Fang, Z. Liu, C. Han, et al., Chem. Commun. 56 (2020) 9158–9161.
[8] X. Chen, X. Li, Y. Peng, et al., Adv. Funct. Mater. 35 (2025) 2416091.
[9] S. Zhao, B. Liu, K. Li, et al., Nat. Commun. 15 (2024) 2970.
[10] X. Chen, M. Ruan, C. Wang, et al., J. Mater. Chem. A 12 (2024) 15440–15452.
[11] G. Fang, Z. Liu, C. Han, et al., ACS Appl. Energy Mater. 4 (2021) 3842–3850.
[12] Y. Zhong, S. Chen, T. Xiao, et al., J. Phys. Chem. Solids 202 (2025) 112691.
[13] J. Zhang, Y. Liu, T. Dittrich, et al., Nat. Commun. 16 (2025) 1515.
[14] G. He, J. Li, W. Qiu, et al., Chem. Eng. J. 469 (2023) 144096.
[15] T.W. Kim, K.S. Choi, Science 343 (2014) 990–994.
[16] X. Ning, P. Du, Z. Han, J. Chen, X. Lu, Angew. Chem. Int. Ed. 60 (2021) 3504.
[17] X. Ning, D. Yin, Y. Fan, et al., Adv. Energy Mater. 11 (2021) 2100405.
[18] L. Xu, M. Li, F. Zhao, et al., Appl. Catal. B: Environ. Energy 359 (2024) 124503.
[19] B. Zhang, X. Huang, Y. Zhang, et al., Angew. Chem. Int. Ed. 59 (2020) 18990–18995.
[20] G. Fang, Z. Liu, C. Han, Appl. Surf. Sci. 515 (2020) 146095.
[21] M. Li, M. Saqib, L. Xu, et al., J. Mater. Chem. A 12 (2024) 19259.
[22] C. Li, S. Mujtaba, J. Quan, et al., Adv. Funct. Mater. 35 (2025) 2501262.
[23] D. Chen, Z. Liu, S. Zhang, Appl. Catal. B: Environ. Energy 265 (2020) 118580.
[24] X. Chen, X. Li, Y. Peng, et al., Adv. Funct. Mater. 35 (2025) 2416091.
[25] Z. Wang, G. Liu, C. Ding, et al., J. Phys. Chem. C 119 (2015) 19607–19612.
[26] H. Niu, L. Gao, M. Liu, et al., Appl. Catal. B: Environ. Energy 358 (2024) 124369.
[27] P. Wang, P. Fu, J. Ma, et al., ACS Catal. 11 (2021) 12736–12744.
[28] Y. Zhang, L. Xu, B. Liu, et al., ACS Catal. 13 (2023) 5938–5948.
[29] L. Zhan, Y. Wang, M. Liu, et al., Chin. Chem. Lett. 36 (2025) 109695.
[30] L. Wang, J. Zhang, Y. Li, et al., Appl. Catal. B: Environ. Energy 336 (2023) 122921.
[31] T. He, Y. Zhao, D. Benetti, et al., J. Am. Chem. Soc. 146 (2024) 27080–27089.
[32] L. Liu, M. Ruan, C. Wang, et al., Appl. Catal. B: Environ. Energy 354 (2024) 124117.
[33] L. Xu, Y. Zhang, B. Liu, et al., ACS Nano 19 (2025) 15863–15875.
[34] J. Ye, C. Li, J. Xu, et al., Adv. Mater. 37 (2025) 2419673.
[35] N. Zhang, Y. Yi, J. Lian, Z. Fang, Chem. Eng. J. 395 (2020) 124897.
[36] M. Li, X. Wang, K. Liu, et al., Adv. Mater. 35 (2023) 2302462.
[37] R. Zhang, X. Ning, Z. Wang, et al., Small 18 (2022) 2107938.
[38] J. Nie, J. Shi, L. Li, et al., Adv. Funct. Mater. 35 (2025) 2414493.
[39] Y. Yan, M. Ouyang, Y. Xing, et al., Appl. Catal. B: Environ. Energy 365 (2025) 124864.
[40] S. Sun, G. Li, S. Zhu, et al., J. Mater. Chem. A 12 (2024) 17463–17470.
[41] S. Kim, M.A. Mahadik, W.S. Chae, et al., Appl. Surf. Sci. 513 (2020) 145528.
[42] Y. Ma, A. Kafizas, S.R. Pendlebury, F.L. Formal, J.R. Durrant, Adv. Funct. Mater. 26 (2016) 4951–4960.